Proposed Design Procedure of a Helical Coil Heat Exchanger for an Orc Energy Recovery System for Vehicular Application

Giacomo Bonafoni, Roberto Capata

Proposed Design Procedure of a Helical Coil Heat Exchanger for an Orc Energy Recovery System for Vehicular Application

Giacomo Bonafoni [1], Roberto Capata [1,a]

1 – Department of Mechanical and Aerospace Engineering, University of Rome Sapienza, Via Eudossiana 18, 00184 Rome, Italy
a – roberto.capata@uniroma1.it

Keywords: Organic Rankine Cycle; energy recovery; energy efficiency in transportation; heat exchanger; helical coiled tube; finite element analysis.

ABSTRACT. There are several systems that produce energy from low grade heat sources such as Stirling engines, thermoelectric generators, and ORC (Organic Rankine Cycle) systems. This paper shows the heat recovery from exhaust gases of a 1400 cc Diesel engine, to vaporize the working fluid of a small (<10 kW) ORC system. The main objective is to have a system as compact as possible, to make it suitable for transport applications such as cars, ships, trains, etc. Three fluids were studied for this application: water and two refrigerant fluids: R134a and R245fa, which were found to be more appropriate than water at certain pressure and temperature values. Afterwards, a design procedure was proposed, then the heat exchanger was modeled and finally a steady-state thermal and structural analysis were carried out using a commercial software to find the temperature and the effects of the thermal stress on the material of the helical coiled tube.

Introduction

Energy recovery systems represent an interesting field of research, because they use the "waste" energy from industrial processes or from energetic processes, to produce other energy; this is a way to improve energy efficiency for a large range of activities such as agriculture, district heating, heavy industry, power plants, marine and land transportation. Different forms of waste energy can be recovered such as kinetic energy (in vehicular applications), electromagnetic energy and thermal energy. The last one is the most interesting because it provides the greatest quantity of energy compared to the others. To recover thermal energy, from low and medium temperature, the most used systems are thermodynamic systems such as the Organic Rankine cycle and Stirling engine. This paper focuses on the ORC technology for vehicular application, which can lead to a considerable increase in engine efficiency, producing extra-power from the waste heat of the exhaust gases of a Diesel engine, in this case. This increase in efficiency also means lower fuel consumption, and direct environmental and economic advantages. Another environmental advantage is the cooling, to which the exhaust gases are subject in the heat exchanger, which avoids the gas discharge at temperatures much higher than that of the environment. However, while the ORC systems are often used for stationary

Nomenclature I

A	Area	m^2
A_{ex}	Thermal exchange surface	m^2
c_p	Isobaric specific heat	J/(kg·K)
d_c	Coiled tube internal diameter	m
D_c	Helix diameter	m
De	Dean number	
D_e	Equivalent diameter shell	m
Δp	Pressure drop	Pa
f, f_s, $f_{tp,s}$	Friction factor, friction factor for a straight tube, two-phase friction factor for a straight tube	
G	Mass velocity	kg/(m^2·s)
h	Convective coefficient	W/(m^2·K)
$HRVG$	Heat Recovery Vapor Generator	
k	Thermal conductivity	W/(m·K)
L	Length	m
$LMTD$	Log mean temperature difference	K
$\dot{m}$	Mass flow	kg/s
N	Number of turns	
Nu	Nusselt number	
p	Pitch	m

applications (solar, biomass, geothermal power plants and combined cycles), it is still difficult to use this technology in the transport sector, due to the complexity and the dimensions of such a system. At present, several important automotive and energetic companies such as BMW, Honda, Cummins, Opcon, Enertime are studying the suitability of the traditional and of the organic Rankine bottoming cycle to increase energy efficiency in cars, trucks, ships and trains [3].

2. The ORC power plant

2.1. Configuration. For minimizing the dimensions and the complexity of the entire system, a direct configuration has been chosen. In this kind of system, the ORC working fluid takes the heat directly from the exhaust gases through a heat exchanger located inside the engine drainpipe. In an indirect configuration, instead, a thermal oil loop is integrated, to avoid a direct contact between exhaust flows and working fluid [4]. The indirect configuration is safer than the direct one, due to the flammability of the ORC working fluids at certain temperature and pressure, but, on the other hand, it requires an oil loop, which means an increase in components and space occupied. Hence, in order to use the direct configuration, non-flammable fluids at the working conditions and high-temperature resistant materials must be used.

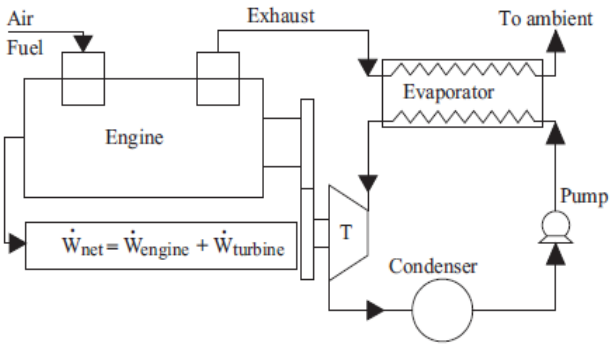

Figure 1. ORC system for heat recovery from engine exhaust gases [2]

2.2. The thermodynamic cycles. The thermodynamic feasibility of the ORC power plant has already been studied in previous research papers [5, 6, 7, 8], thus the cycles were analyzed with the aim of finding out input and output data of each component of the entire system, and of choosing the most efficient cycles (and discarding the less efficient). First, the thermodynamic cycle has been studied and then developed with the software CAMEL-Pro Simulator, to simulate the energy

Nomenclature II

Pr	Prandtl number	
Q	Thermal power	W
q	Heat flux	W/m^2
r	Radius	m
Re	Reynolds number	
T	Temperature	K
T_h, T_c	Hot and cold fluid temperature	K
$T_{w,in}$, $T_{w,ex}$	Internal and external wall temperature	K
u	Velocity	m/s
U	Thermal transmittance	W/(m^2·K)
V	Volume	m^3
W_t	Thermal power transmitted	W
x	Vapor quality	
ε	Void fraction	
μ	Viscosity	Pa·s
ρ	Density	kg/m^3
χ_{tt}	Martinelli turbulent-turbulent number	

A	Available
B	Boiling
C	Coil
E	External
G	Gas
I	Internal
In	Inlet
L	Liquid
Lo	Liquid-only
Max	Maximum
Min	Minimum
Out	Outlet
S	Shell
Tp	Two-phase
V	Vapor

conversion process. Many comparisons between various fluids have been carried out in several previous researches, with different results, due to the different applications, that depending on the available heat source, on plant working temperatures and pressures [9,10]. In this paper three different fluids were preliminarily studied: water, R134a and R245fa. Main data for the exhaust gases (the hot source) from the Diesel engine and for the cooling water (the cold sink which, for both land and marine vehicular application, may be the vehicle cooling circuit) are shown in Table 1 and Table 2. The other data (enthalpy, thermal conductivity, density, viscosity, etc.) of gas, water and working fluids has been provided by FluidProp (Microsoft Excel extension), NIST [11] and Peacesoftware [12] databases. The values of cycles efficiencies in Table 3 may seem quite low compared to "conventional" theoretical efficiencies calculated for the Rankine and Organic Rankine Cycle. This is because, in this first simulation, a turbine efficiency of 85%, a pump efficiency of 90% and heat losses of 10% were assumed, with the aim of obtaining a cycle as realistic as possible. In fact, existing models present experimentally calculated efficiencies which are very similar to the values obtained in Table 3. One can immediately notice that the water cycle has the lowest thermodynamic efficiency and provides the lowest mechanical power output, so this cycle will be discarded. The best cycle in terms of power output and theoretical efficiency is the R245fa cycle. In Figure 3, an example of an ORC system is provided. The numbers represent the incoming and outgoing flows of each component. Number 1 is the mechanical power output from the turbine. Regarding the working fluid, number 2 is the outlet from the HRVG and the inlet in the turbine while number 3 represents the outlet from the turbine and the inlet in the condenser. Number 4 is the outlet from the condenser and the inlet in the pump, number 11 is the outlet from the pump and number 10 is the inlet in the HRVG (it is separated to better check the inlet and outlet flow in the HRVG and to check the process itself). Instead, number 9 represents the mechanical power used by the pump, numbers 7 and 8 represent the inlet and outlet of the exhaust gases in the HRVG, and finally, numbers 6 and 5 are the inlet and outlet of the cooling water in the condenser.

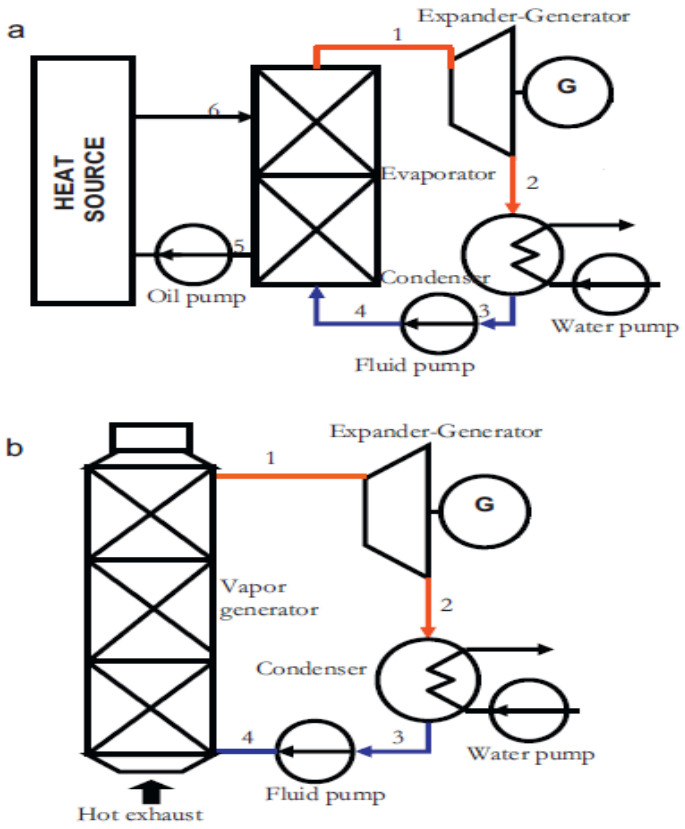

Figure 2. Indirect (a) vs direct (b) configuration

Table 1. Thermodynamic data for the exhaust gas

Mass flow (kg/s)	**Temperature (K)**	**Pressure (kPa)**	**Enthalpy (kJ/kg)**	**C_p (kJ/(kg*K))**	**Thermal Cond. (W/(m*K))**	**Density (kg/m^3)**	**Viscosity (Pa*s)**
0.15	845.15	200	1031.153	1.109	0.0596	0.824	$3.86*10^{-5}$

Table 2. Main data for the cooling water for the three different cycles

	Mass flow (kg/s)	**Temperature (K)**	**Pressure (kPa)**
R134a	1	288,15	150
R245fa	0,7	288,15	150
Water	0,4	288,15	150

In Table 3, the main parameters and the results of the simulations are also shown.
Table 4 shows the ideal thermal power for the counter flow heat exchanger, sub-divided in its three parts: pre-heater, vaporizer, super-heater for each fluid. The partition of the heat exchanger was made using the same software. The state points in figure 4 represent the flows of the working fluid and exhaust gas in each heat exchanger part: point 1 represents the working fluid inlet (in liquid state) in the pre-heater, 2 is the fluid outlet from the pre-heater and, at the same time, its inlet in the evaporator. Point 3 is the outlet of the fluid (now in the state of saturated vapor) from the evaporator and the inlet in the super-heater and point 4 is the outlet of the super-heated vapor from the heat exchanger. For the exhaust gases, 5 is the inlet in the super-heater, point 6 is the outlet from the super-heater and the inlet in the evaporator (remembering that the heat exchanger is a counterflow device); 7 is the outlet from the evaporator and the inlet in the pre-heater, and 8 is the outlet from the pre-heater. In table 5, the inlet and outlet temperatures and ideal working pressures are shown, without losses in the heat exchanger for the working fluids and the exhaust gases.

Table 3. Results of the thermodynamic simulations

	R134a	**R245fa**	**Water**
Mass flow rate (kg/s)	0.38	0.35	0.032
Turbine work (kJ/kg)	8.746	13.011	65.296
Pump work (kJ/kg)	0.702	0.378	0.152
Boiler heat (kJ/kg)	188.948	206.712	2307.912
Condenser heat (kJ/kg)	180.904	193.772	2242.768
Max. temperature (K)	333	345	433
Min. Temperature (K)	307	313	386
Max. Pressure (kPa)	1500	612	310
Min. Pressure (kPa)	950	300	210
Carnot cycle efficiency (%)	7.8	9.28	10.85
Cycle efficiency (%)	**4.63**	**6.29**	**2.83**
Mechanical power output P_t-P_p (kW)	**3.06**	**4.42**	**2.08**

Table 4. Thermal power of the sub-components of the heat exchanger for R134a and R245fa cycles

Thermal power (kW)	**Pre-heater**	**Vaporizer**	**Super-heater**
R134a	12.951	55.783	1.935
R245fa	14.758	56.393	0.536

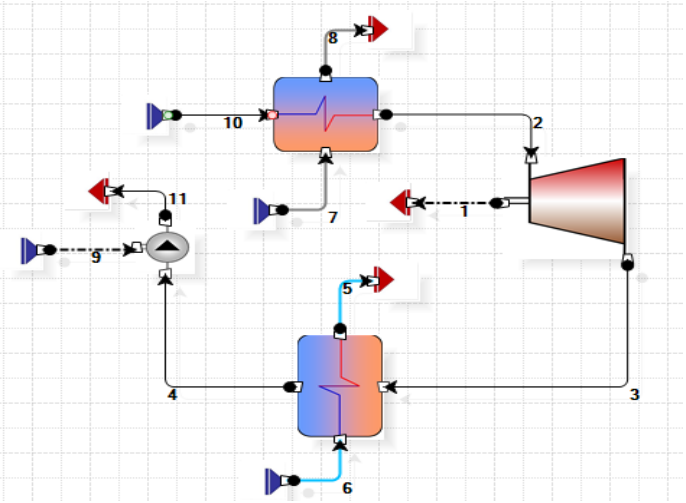

Figure 3. Example of an ORC system developed on Camel-PRO Simulator

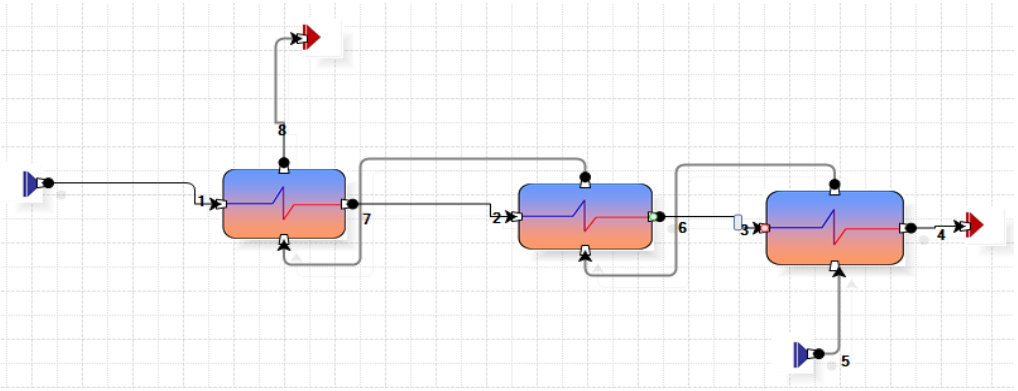

Figure 4. Partition of the counterflow heat exchanger into 3 sub-components

*Table 5. Temperature, pressure and steam quality in each part of the heat exchanger for R134a (4a) and R245fa (*4b) cycles

R134a	**Pre-heater**	**Vaporizer**	**Super-heater**
T inlet (K)	307	328.202	328.202
T outlet (K)	328.202	328.202	333
Pressure (kPa)	1500	1500	1500
Exhaust Gas			
T inlet (K)	487.465	833.599	845.15
T outlet (K)	403.507	487.465	833.599
Pressure (kPa)	200	200	200
R245fa	**Pre-heater**	**Vaporizer**	**Super-heater**
T inlet (K)	313	343.45	343.45
T outlet (K)	343.45	343.45	345
Pressure (kPa)	612	612	612
Exhaust Gas			
T inlet (K)	492.54	841.95	845.15
T outlet (K)	396.864	492.542	841.95
Pressure (kPa)	200	200	200

3. The Heat Recovery Vapor Generator (HRVG): proposed engineering design procedure of the helical coil heat exchanger

To achieve the maximum thermal exchange in the minimum volume (so a high rate A_{ex}/V) with a simple structure, the choice of the configuration fell to a shell and coiled tube heat exchanger. Due to its shape, in fact, for an equal shell's length, a coil presents a larger surface of thermal exchange than a straight tube, or even a U-tube. The space limitations for the heat exchanger design can be summarized as such: the maximum length of the entire heat exchanger must not exceed 1 meter and the maximum diameter must not exceed 30 centimeters. The package size of the turbine designed for the cycle [13], instead, is about 25x25 cm. There are different procedures for the design of this type of exchangers, often apply for certain temperatures and flow rate range, or for different working fluids. Several authors [14,15,16,17,18] have interpreted the mass flow rate, both monophasic or biphasic, introducing various dimensionless coefficients, and the various procedures for the calculation of various fractions or mixture composition. Similarly, the heat exchange has been evaluated according to their assumptions and reviews, often confirmed and validated by experimental tests. In this study the authors tried to realize, and then to propose a methodology and a procedure, which is not new, of course, but that may have general validity or a wider application range more than those described by various authors.

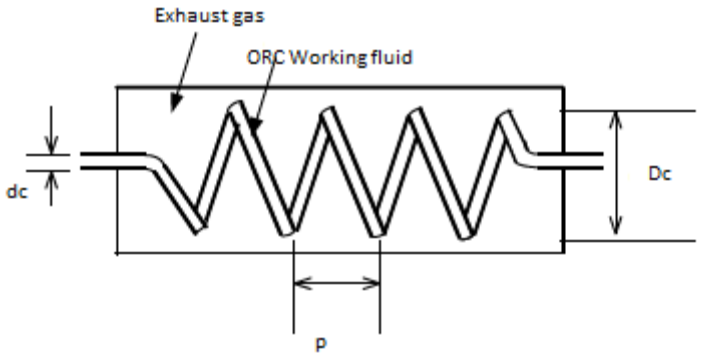

Figure 5. Schematic view of typical shell and coiled tube heat exchanger

In the design the heat exchanger, the first step is to sub-divide it in three parts: the pre-heater, the vaporizer, the super-heater. The thermal power required for all three sections and for the different working fluids to be tested are known, along with temperatures and pressures of the input and output exhaust gas and liquid/steam. It is an iterative procedure:
1) in the first iteration, the pressure is assumed constant
2) calculate the heat exchanger dimensions
3) evaluate the pressure drops.
With the obtained pressure drops values, iterations have been carried out until convergence is reached. The first step for the design of the entire heat exchanger is the super-heater design (for the R245fa and R134a fluid, it has just the necessary length to ensure the complete evaporation of the fluid and a little superheating).

3.1 Super-heater design. Shell-side: exhaust gas
Coil-side: single-phase working fluid (vapor)
To design it, it is necessary to impose the values for the velocity u of the two fluids and the Reynolds number on both the shell and coil sides.

3.1.1 Shell-side. Inlet and outlet temperatures and pressure of the exhaust gases are known, so the relative values of ρ, μ, k and c_p (and consequentially their average values) can be easily obtained.

$$\dot{m} = \rho A u \tag{1}$$

Imposing $u \leq 40m/s$ the equivalent diameter is found:

$$D_e = \sqrt{4\,\dot{m}/\pi\rho u} \tag{2}$$

Hence, the Reynolds number:

$$Re = \frac{\rho u D_e}{\mu} \tag{3}$$

The gas Prandtl number:

$$Pr = \frac{c_p \mu}{k} \tag{4}$$

The Nusselt (turbulent) number i [16]:

$$Nu = 0{,}023 Re^{0.8} Pr^{0.4} \tag{5}$$

And finally the coefficient of convective heat transfer shell-side:

$$h_s = \frac{Nu \cdot k}{D_e} \tag{6}$$

3.1.2 Coil-side

Inlet and outlet temperatures and working pressure of the superheated vapor are known. Consequently, the relative values of viscosity (μ), density (ρ), isobaric specific heat capacity (c_p) and thermal conductivity (k), can be obtained from databases and finally their average values can be calculated. The inside diameter of the tube being fixed, and knowing the mass flow (ṁ) and the average density of the fluid, the (average) velocity u (this value must be less than 30 m/s) can be computed:

$$u = \dot{m}/(\rho A) \tag{7}$$

Where

$$A = \pi {d_c}^2/4 \tag{8}$$

Then, it is possible to calculate the Reynolds and Prandtl numbers for the fluid. Having also fixed the coil diameter D_c, the critical Reynolds number (transition laminar/turbulent flow) for a helical tube is (in this work the flow regime is always turbulent):

$$Re_c = 2000\left(\frac{d_c}{D_c}\right)^{0.32} \tag{9}$$

Number of Dean (Reynolds "adapted" to helical tubes considering the effects of the centrifugal forces on the flux):

$$De = Re(\frac{d_c}{D_c})^{1/2} \tag{10}$$

The turbulent Nusselt number (the flow conditions, in this work, are always turbulent):

$$Nu = 0.023Re^{0.85}Pr^{0.4}(\frac{d_c}{D_c})^{0.1} \tag{11}$$

And finally h_{coil} :

$$h_c = \frac{Nu \cdot k}{d_c} \tag{12}$$

3.1.3. Heat Exchanger analysis

The total thermal power is:

$$Q_s = \dot{m}_g c_{p,g}(T_{g,in} - T_{g,out}) = Q_c = \dot{m}_v c_{p,v}(T_{v,in} - T_{v,out}) \tag{13}$$

And also:

$$Q = UA \cdot LMTD \tag{14}$$

where LMTD – is the logarithmic mean temperature difference, which, for a counter flow heat exchanger is:

$$LMTD = \frac{(T_{g,out} - T_{v,in}) - (T_{g,in} - T_{v,out})}{(ln((T_{g,out} - T_{v,in})/(T_{g,in} - T_{v,out}))} \tag{15}$$

The overall thermal transmittance is:

$$\frac{1}{U} = \frac{A_e}{h_i A_i} + \frac{A_e \ln(d_e/d_i)}{2\pi k L_c} + \frac{1}{h_e} \tag{16}$$

Where A_e, d_e and L_c – are the heat exchange area (external surface of the coil), the external diameter and the coil length, and A_i and d_i are the internal surface of the coiled tube and the internal diameter; k is the thermal conductivity of the material:

$$A = \pi d L_c \tag{17}$$

The exchange surface can be determined:

$$A = Q/(U \cdot LMTD) \tag{18}$$

And finally, the coil's length L_c, which is also (where R_c is the helix radius and p the pitch, previously fixed):

$$L_c = N\sqrt{(2\pi R_c)^2 + p^2} \tag{19}$$

The number of turns of the coil N is so calculated from this expression.

Finally, the shell's length L_s:

$$L_s = p \cdot N \tag{20}$$

Coil volume:

$$V_c = \frac{\pi d_c^2}{4} \cdot L_c \tag{21}$$

Volume available for the gas:

$$V_a = {D_e \pi d_e Lc}/{4} \tag{22}$$

Shell volume:

$$V_s = V_c + V_a \tag{23}$$

In details:

$$V_s = \frac{\pi D_s^2}{4} \cdot L_s \tag{24}$$

From this equation, the diameter of the shell D_s is finally computed.

3.1.4. Friction factors and pressure drops

Coil:

Turbulent friction factor:

$$f_c = f_s \left[Re \left({d_c}/{D_c} \right)^2 \right]^{1/20} \tag{25}$$

where

$$f_s = 0.046(Re)^{-0.2} \tag{26}$$

Then pressure drop is calculated:

$$\Delta p = \frac{2 f_c \rho L_c u^2}{d_c} \tag{27}$$

Shell:

Turbulent flow

$$f_s = 8 \cdot 0.023(Re)^{-0.2} \tag{28}$$

Pressure drop:

$$\Delta p = \frac{f_s \rho L_s u^2}{2 D_e} \tag{29}$$

3.2. Vaporizer design

3.2.1. Shell –side. The procedure for the shell design is the same already discussed in 3.1.1

3.2.2. Coil –side. During the phase change, different formulations have been used to find the dimensionless coefficients for the description of flow and heat exchange. For a more accurate calculation, the evaporator is subdivided in two parts: in the first the vapor quality is between 0 and 0,5 and the second between 0,5 and 1. For both the two parts, the procedure can be listed as below. First, calculate Martinelli's number [16] for turbulent-turbulent flow:

$$\chi_{tt} = (\frac{1-x}{x})^{0.9}(\frac{\rho_v}{\rho_l})^{0.5}(\frac{\mu_l}{\mu_v})^{0.1} \tag{30}$$

The liquid-only Reynolds and Nusselt numbers and the convective heat transfer coefficient (calculated if all the flow was liquid, i.e. x=0) are:

$$Re_{lo} = \frac{\rho_l u_{lo} d_c}{\mu_l} \tag{31}$$

$$Nu_{lo} = 0.023 {Re_{lo}}^{0.85} {Pr_l}^{0.4} (\frac{d_c}{D_c})^{0.1} \tag{32}$$

$$h_{lo} = \frac{Nu_{lo} \cdot k}{d_c} \tag{33}$$

Finally, the boiling convective heat transfer coefficient is calculated:

$$h_b = 2.5 h_{lo} ({}^{1}/_{\chi_{tt}})^{0.75} \tag{34}$$

3.2.3. Heat Exchanger analysis

The same procedure as above with the difference that, in the heat balance, in order for the fluid to be heated, there is a difference in enthalpy (latent heat of vaporization) instead of a difference in temperature.

$$Q_s = \dot{m}_g c_{p,g} (T_{g,in} - T_{g,out}) = Q_c = \dot{m}_{l-v} (h_{out} - h_{in}) \tag{35}$$

And

$$Q = UA \cdot LMTD \tag{36}$$

$$LMTD = \frac{T_{g,out} - T_{g,in}}{(ln((T_{g,out} - T_{l-v,in})/(T_{g,in} - T_{l-v,out}))} \tag{37}$$

3.2.4. Friction factors and pressure drops

In this situation, the computation of the friction factors is different from the single-phase zone. Here the Kim correlation [16] is used. Calling *x* the vapor quality, viscosity, density and velocity of the fluid for x = 0 and x = 1 are known. So the void fraction ε, which represents the cross sectional area occupied by the vapor phase in respect to the total sectional area, can be computed:

$$\varepsilon = \frac{A_v}{A_v + A_l} \tag{38}$$

Butterworth developed a generalized equation for it, and here Thome's model [16] for the exponents is used:

$$\varepsilon = \left[1 + \left(\frac{1-x}{x}\right)\left(\frac{\rho_v}{\rho_l}\right)^{0.84}\left(\frac{\mu_l}{\mu_v}\right)^{0.8}\right]^{-1} \tag{39}$$

The density and viscosity of the two-phase mixture are calculated:

$$\rho_{tp} = \rho_v \cdot \varepsilon + \rho_l(1-\varepsilon) \tag{40}$$

$$\mu_{tp} = \rho_{tp}\left[\frac{x \cdot \mu_v}{\rho_v} + \frac{(1-x)\mu_l}{\rho_l}\right] \tag{41}$$

Now the friction factor for a straight pipe and for a coiled pipe (Kim) can be found [16]:

$$f_{tp,s} = 0.079\left(\frac{G \cdot d_c}{\mu_{tp}}\right)^{-0.25} \tag{42}$$

where *G* – is the two-phase mass velocity:

$$G = x\rho_v u_v + (1-x)\,\rho_l u_l \tag{43}$$

$$f_{tp,c} = f_{tp,s}\left[1 + Re_{lo}\left(\frac{d_c}{D_c}\right)^2\right]^{1/20} \tag{44}$$

The pressure drop in the boiler is:

$$\Delta p = \frac{2 f_{tp,c} G^2 L_c}{\rho_{tp} d_c} \tag{45}$$

3.3. The pre-heater design

The procedure is the same already discussed for the superheater, both for the shell and the coil, with the obvious difference that the fluid to be heated is in a liquid state. Same considerations for friction factor and pressure drop calculations.

3.4. Successive iterations

With the values of pressure drop it is possible to continue with a second iteration, increasing the inlet pressure of each sub-part of the heat exchanger. The pump must be capable to satisfy the extra pressure request. After re-calculating the length of the heat exchanger, the computation of the pressure drop is repeated until convergence is reached.

3.5. Efficiency of the heat exchanger

The efficiency is defined as the ratio between the thermal power actually transmitted and the thermal power theoretically transmittable. The second term is derived by the difference of temperature reached by the fluid with the lower thermal flow rate C_{min} (product of specific heat and mass flow) if the (counter flow) heat exchanger had infinite length [19].

$$\varepsilon = \frac{W_t}{W_{t,max}} = \frac{W_t}{C_{min}(T_{h,in} - T_{c,in})} \tag{46}$$

3.6. Final Results

Below the design results for both R134a and R245fa HRVG are shown.

Table 6. Final results of the design procedure for both R134a (5a) and R245fa (5b) HRVG

R134a	**Preheater**	**Boiler $0 \leq x \leq 0.5$**	**Boiler $0.5 \leq x \leq 1$**	**Superheater**
Q (W)	3409.52	6891.9	6891.9	483.848
Length of 1 coil (m)	3.96	3.65	2.21	0.12
N° of turns 1 coil	15.7	14.5	8.7	0.47
Shell length (m)	0,3582	0.3298	0.1996	0.0107

R245fa	**Preheater.**	**Boiler $0 \leq x \leq 0.5$**	**Boiler $0.5 \leq x \leq 1$**	**Superheater**
Q (W)	4158.26	6818	6818	134.156
Length of 1 coil (m)	5.3532	3.7127	2.2151	0.034
Number of turns 1coil	21.2	14.71	8.77	0.13
Shell length (m)	0.4836	0.3354	0.2001	0.003

The table below refers only to the coil-side pressure drops; shell-side losses have been neglected due to their low values (equal or less than 1 kPa). Finally, in table 8, all dimensions are listed.

Table 7. Pressure drops

Pressure drops (kPa)	**R134a**	**R245fa**
Pre-heater	6	6,5
Boiler	35	55
Super-heater	Neglected (<1kPa)	Neglected (<1kPa)

Table 8. Heat Exchangers Final Dimensions

	R134a	**R245fa**
Int. Diam. 1 Coil (m)	0.008	0.008
Ext. Diam. 1 Coil (m)	0.0104	0.0104
Helix diam. (m)	0.08	0.08
Pitch (m)	0.0228	0.0228
Int. Diam. 1 Shell (m)	0.106	0.106
Number of turns (1 coil)	40	46
Total length 1 coil (m)	10.094	11.608
Total length 1 shell (m)	0.9234	1.0602
Total thermal power (kW)	70.71	71.71
Efficiency ε (%)	82.4	84.5

The results show that, even if the R245fa cycle presents the best thermodynamic efficiency and the higher heat exchanger efficiency, the R134a heat exchanger presents a total length of 92.3 cm (14 cm less than the R245fa HRVG length). This value, in addition to economic considerations (R134a is cheaper than R245fa), make the R134a cycle more interesting for this application, so it has been definitively chosen as working fluid. In the following figure, a 3D view is provided, and a possible component assembly.

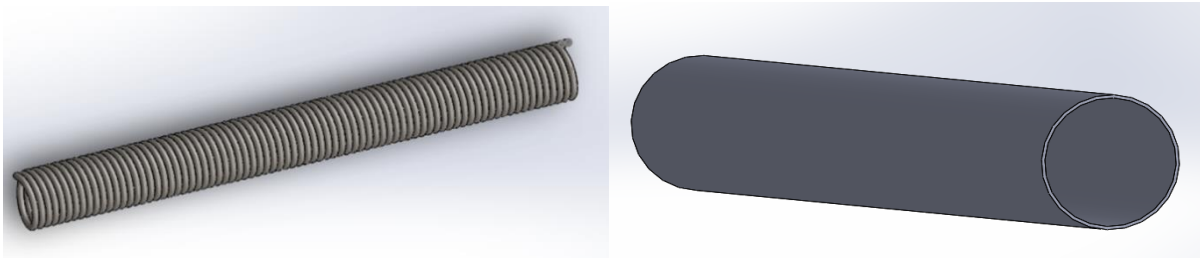

Figure 6 and 7. 3-D view of the two coils and of the shell (R134a)

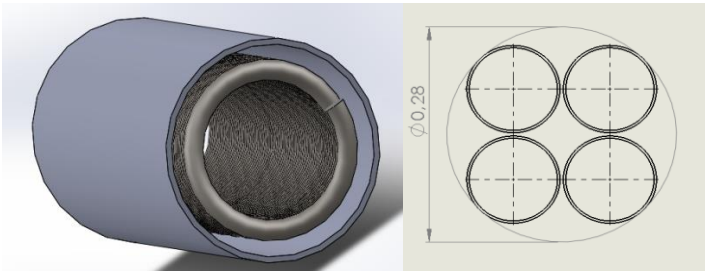

Figure 8 and 9. Assembly of the components and disposition of the four shells with the total occupied diameter (27.6 cm rounded up to 28 cm)

4. The thermal and the structural simulation

4.1 Average wall temperatures. First of all, the average wall temperatures from the heat balance equation were roughly found and then a steady-state thermal simulation was implemented, to check the actual temperature trend inside the thickness of the tube, and at the wall more accurately.
From the heat balance:

$$q = \frac{Q}{A_{ex}} = U(T_h - T_c) \tag{47}$$

q is the heat flux from the hot to the cold fluid and U the overall thermal transmittance, while T_h and T_c are the average temperatures for the hot and cold fluids in each part of the heat exchanger. So, the average heat flux and the temperature at the internal and external diameters of the tube is:

$$q_i = \frac{Q}{A_i} = h_c(T_{w,in} - T_c) \tag{48}$$

$$q_e = \frac{Q}{A_e} = h_h(T_h - T_{w,ex}) \tag{49}$$

In the previous formulas h_h and h_c are the convective coefficients for the hot and cold fluids. Once the thermal transmittance and T_c and T_h are known, the heat flux, in each part of the heat exchanger is computed, as shown in Table 9.

Table 9. Average heat flux from the heat balance

R134a	Ext. Heat flux (W/m^2)	Int. Heat flux (W/m^2)
Pre-heater	13460.24	17498.31
Boiler (0<x<0.5)	30354.97	39461.47
Boiler (0.5<x<1)	48698.95	63308.63
Super-heater	61847.8	80402.15

The values of h_h and h_c, allow to calculate the wall temperatures are: this is a first indication of the temperatures of every part of the coiled tube.

Table 10. Average wall temperatures

R134a	External diameter average temperature (°C)	Internal diameter average temperature (°C)
Pre-heater	51.85	51.5
Boiler (0<x<0.5)	61.77	60.98
Boiler (0.5<x<1)	58.9	57.64
Super-heater	87.21	85.59

4.2 The Steady-State Thermal Simulation

All simulations were conducted using the ANSYS software. However, checking the program library, a modification/insertion was necessary. The AISI 446 stainless steel, with its properties [20], has been inserted into the materials database of ANSYS, and then the geometry was imported from SolidWorks. The next step has been the mesh generation. The most important features chosen for each sub-component of the heat exchanger are (from all available in the software):

- Relevance center: Medium
- Smoothing: Medium
- Transition: Fast
- Span angle center: Medium

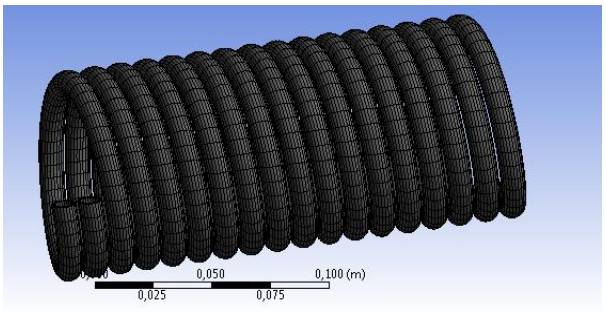

Figure 10. Example of a complete mesh

In the table below the number of nodes and of elements, resulting from the mesh configuration of every single part of the heat exchanger, is illustrated.

Table 11. Number of nodes and elements of the mesh for the steady-state thermal simulation

	Nodes	**Elements**
Pre-heater	204048	30544
Boiler 0-0,5	94088	16204
Boiler 0,5-1	106848	17224

Besides, the values of convective coefficients (considered constant) and temperatures (with an approximated linear trends along the axis) of refrigerant and exhaust were set.

The "boundary conditions" for the simulation are as follows. Once the temperature filed is determined, starting from the HRVG outlet section, it sets the output temperature of the organic fluid of the HRVG superheated section. So, the SH inlet conditions (calculated in the above section) becomes the outlet condition for the vaporizer section, and so on. The other assumed quantity is the fluid mass flow rate and the two convective coefficient (cold side and hot side), computed as previously described.

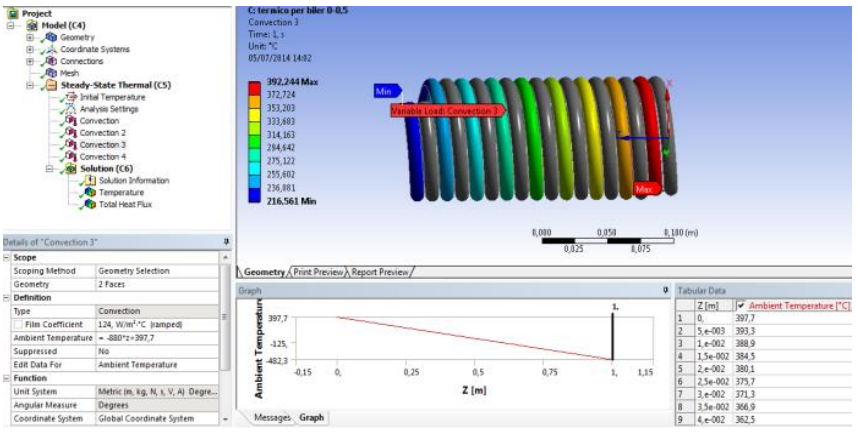

Figure 11. Example of thermal load applied to the geometry

4.3 Results of the thermal simulation and comments

In the following figures, the steady-state thermal study results for the temperature and the heat flux reached by the material for each part of the R134a helical coiled tube are shown:

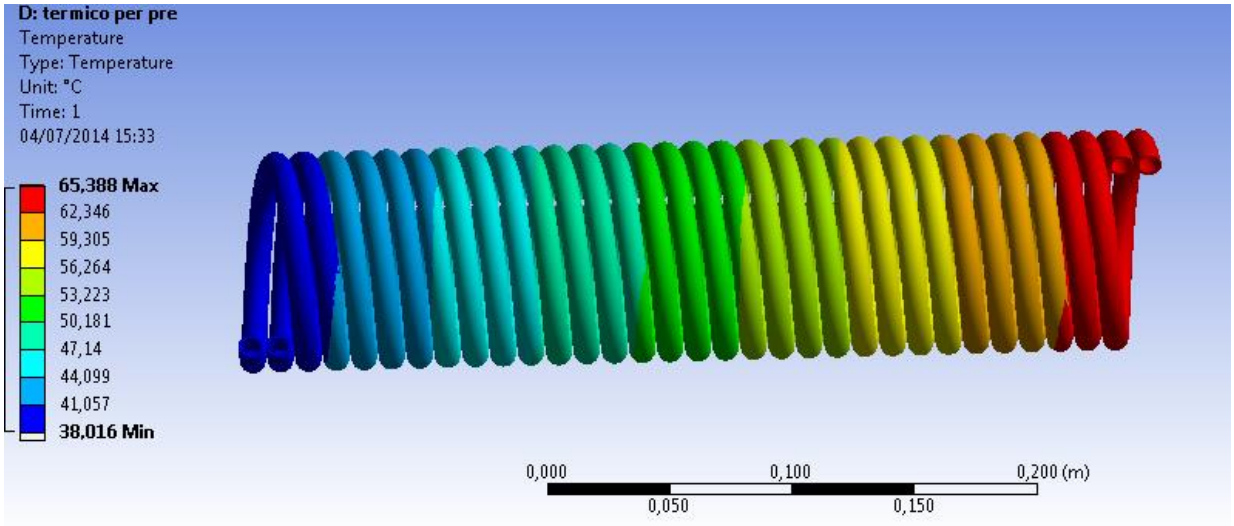

Figure 12 (a). Temperature trend along the pre-heater (°C)

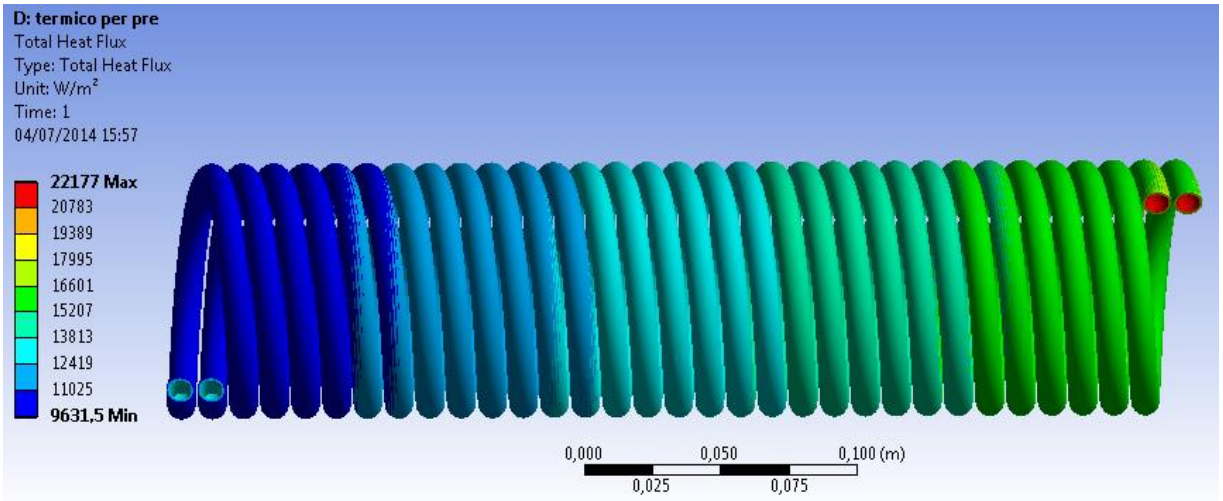

Figure 12 (b). Heat flux trend along the pre-heater (W/m^2)

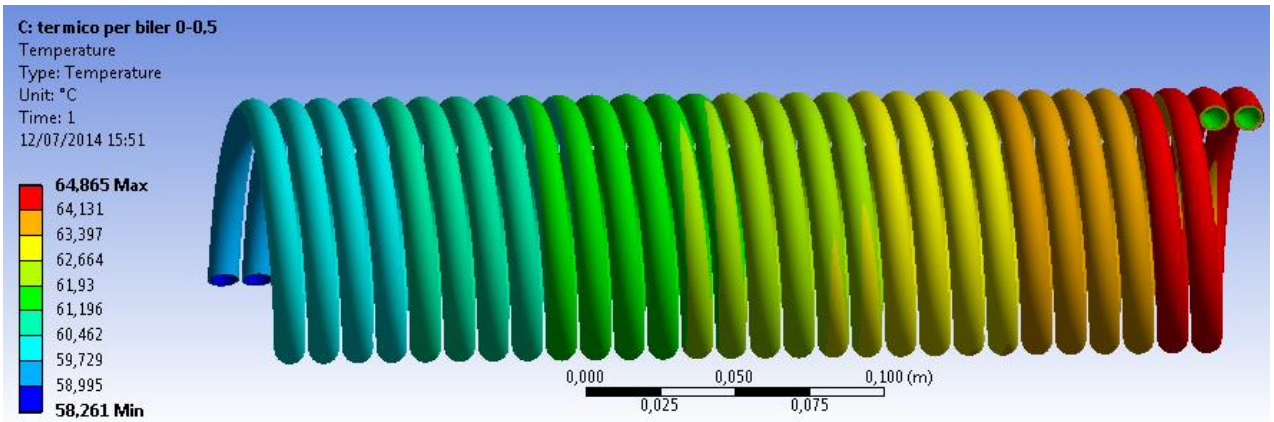

Figure 13a. Temperature trend along the first part of the boiler (0≤x≤0.5)

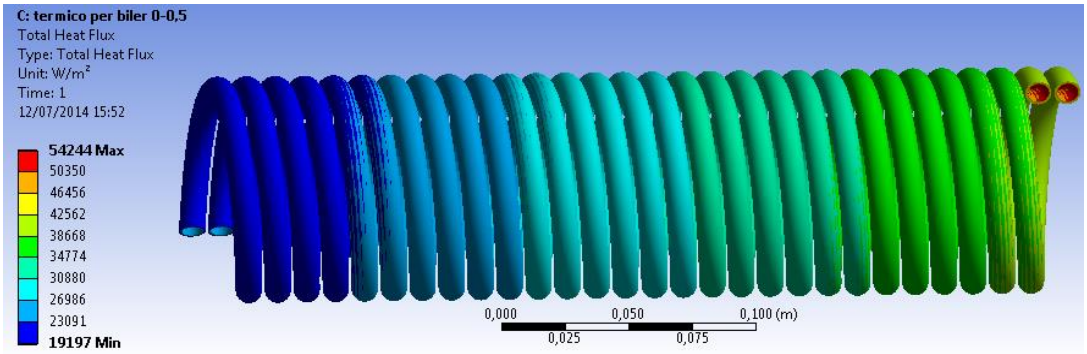

Figure 13b. Heat flux trend along the first part of the boiler (0≤x≤0.5)

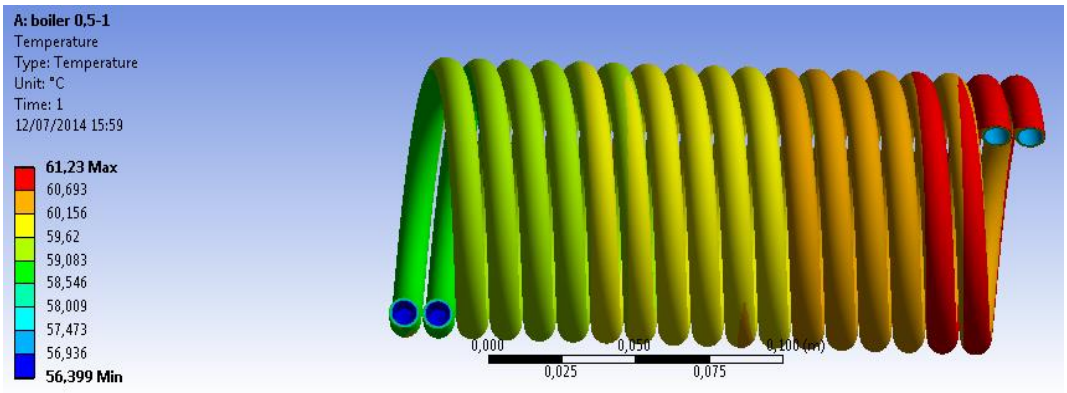

Figure 14a. Temperature trend along the second part of the boiler (0.5≤x≤1)

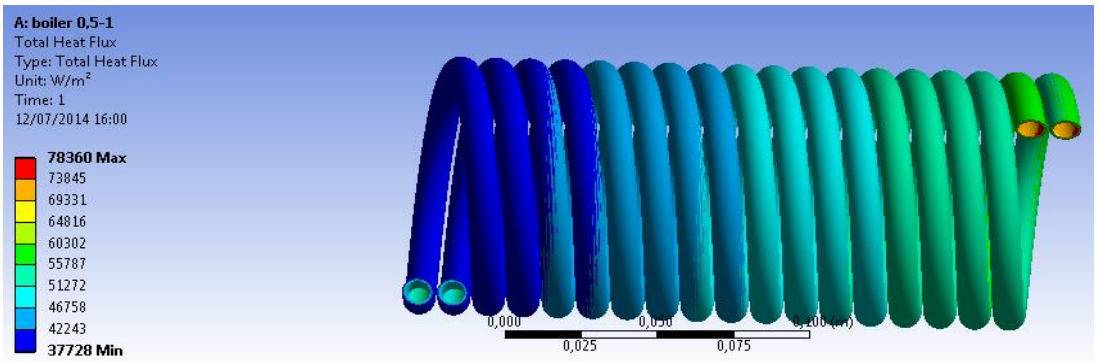

Figure 14b. Heat flux trend along the second part of the boiler (0.5≤x≤1)

The results indicate that the tube temperature is close to the temperature of the refrigerant. The maximum temperature reached on the external surface is 65.4 °C (Figure 12a). This depends on the difference between the flows convective coefficients on inside and outside surface of the tube (inside the order of magnitude is 103-104, outside 102). The simulation of the super-heater has not been implemented due to its very small length (less than 0.5 number of turns of the coiled tube).

4.4 The static structural simulation

For the structural study, the most important mechanical properties of the AISI 446 [20] were added in the Engineering Data, as previously described. The geometry and the mash used is the same used for the thermal simulation. The tablle below shows the numbers of nodes and elements used in the calculation.

Table 12. Number of nodes and elements of the mesh for the static structural simulation

	Nodes	Elements
Pre-heater	208040	31020
Boiler 0-0.5	96048	17104
Boiler 0.5-1	108264	18922

The external temperature field, previously determinate, has been set as "boundary condition". To act in safety conditions, the thermal load, so calculated, was applied to the entire body of the coil. Consequently, the thermal load on the internal surface was overestimated, but accepted. In fact, the program does not allow to set different temperatures on different faces, but only one temperature for the entire body. The second "boundary conditions" concern the pressure. It has been applied on the internal surface, decreased by the external pressure value.

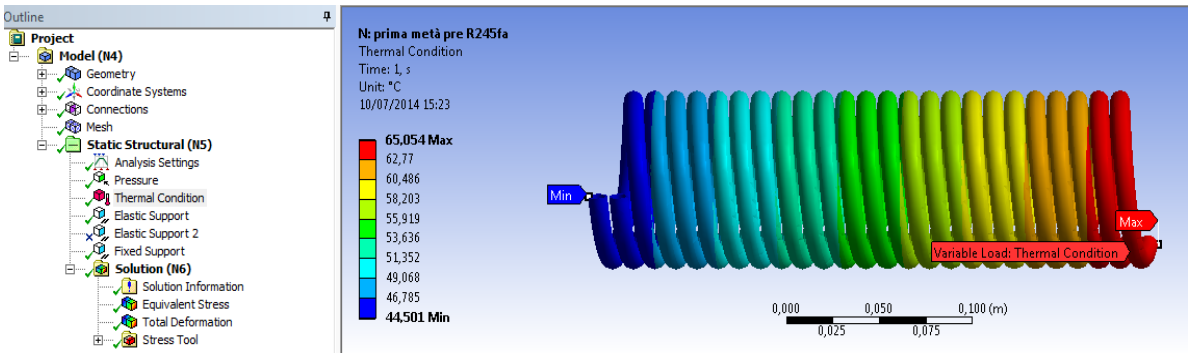

Figure 15. Example of an applied thermal load

All the sub-components of the heat exchanger were bonded to both ends with an elastic support (as suggest by program manual) made of the same material. For the inlet pre-heater and the outlet super-heater, a fixed support has been considered.

4.5. Results of the structural simulation and comments

The following figures show the total deformation of the coiled tubes and the stress safety factor, defined as the yield stress of the material divided by the equivalent stress actually computed in the simulation σ_s/σ. The results indicate that the material tensions stress are always below the yield stress value, thanks to the low operating temperature and pressure. The maximum level is reached at the end of the exchanger, where the fixed supports are used. But, also in this case, the value is far from the limit value. with a safety factor of 4.5 (see figure 16b). The thermal deformations, as stress one, is low, of the order of millimeter. However, the structural simulation only covers the different parts of the coil itself. So, even if the coil doesn't present problems, a study of the thermal effects on the welded junctions between the coiled tube and the shell will be necessary, where stress concentrations are located. Finally, these values has to be checked by an experimental campaign.

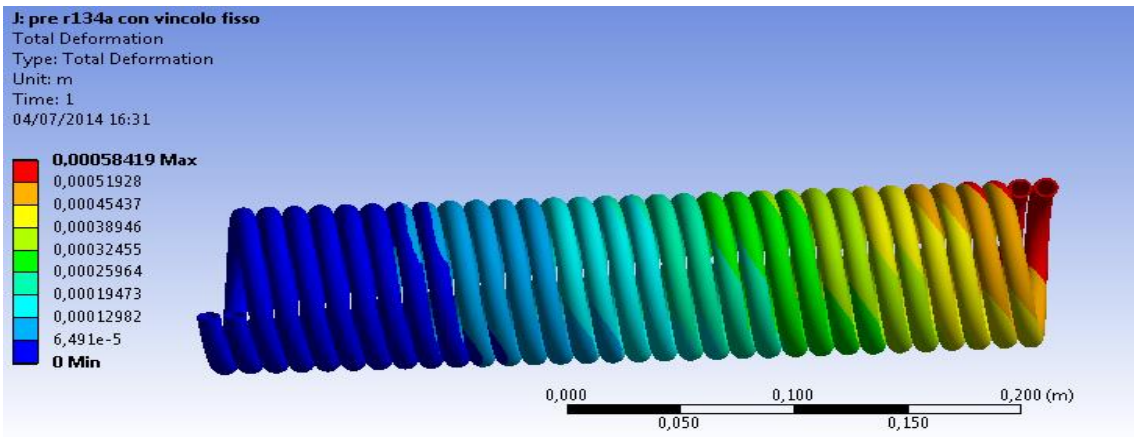

Figure 16a. Total deformation of the pre-heater (m)

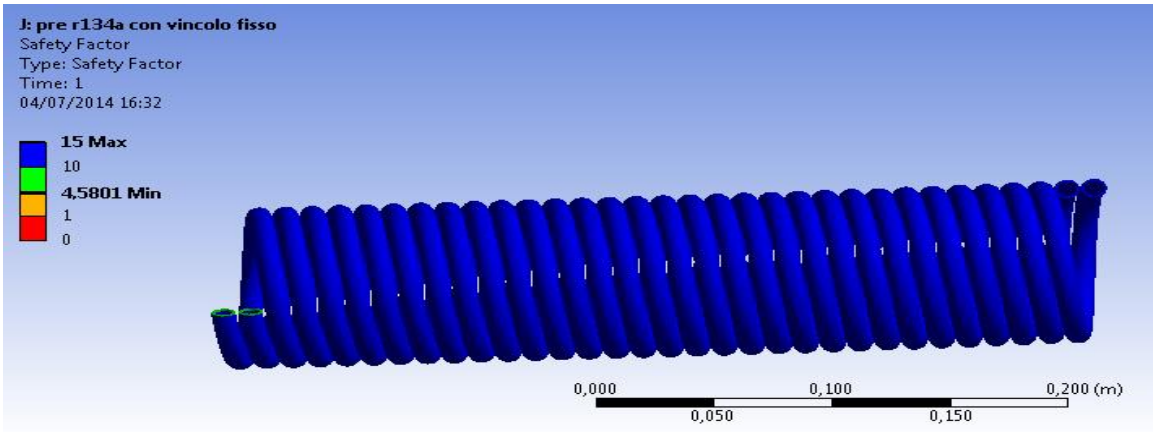

Figure 16b. Safety factor of the pre-heater

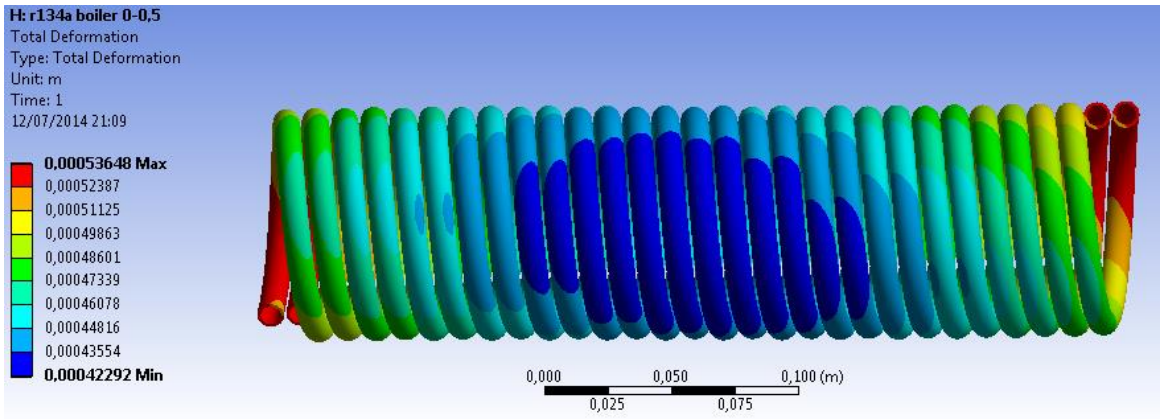

Figure 17a. Total deformation of the first part of the boiler(0≤x≤0.5)

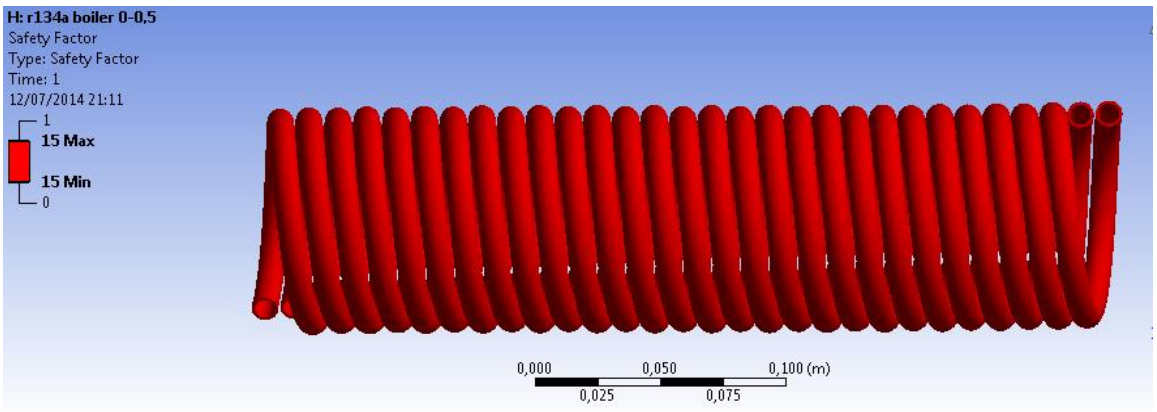

Figure 17b. Safety factor of the first part of the boiler (0≤x≤0.5)

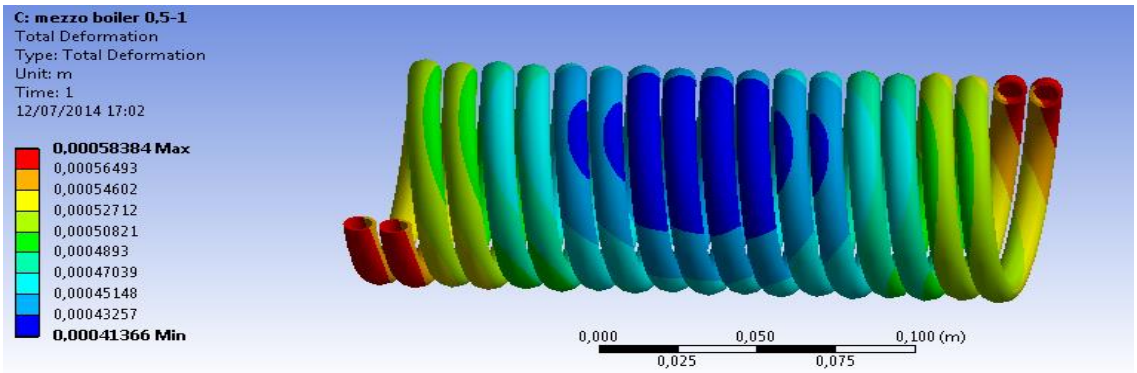

Figure 18a. Total deformation of the second part of the boiler (0.5≤x≤1)

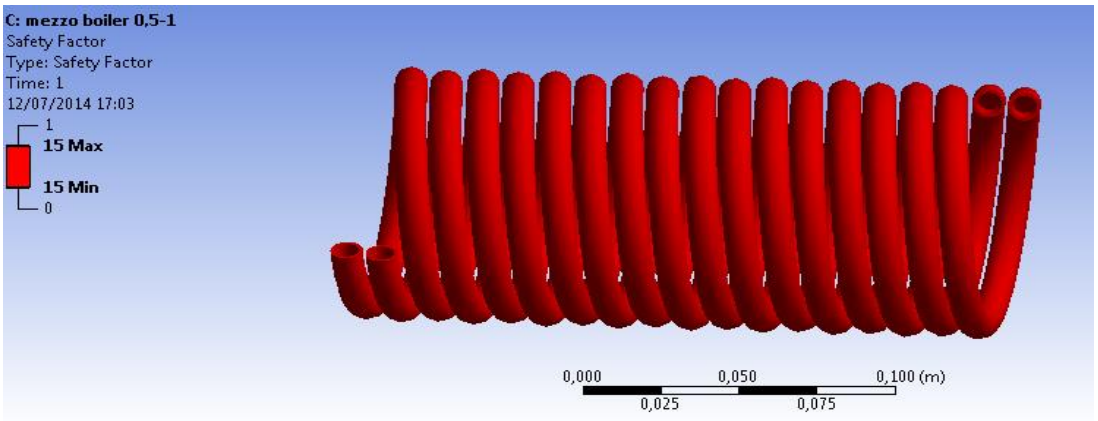

Figure 18b. Safety factor of the second part of the boiler (0.5≤x≤1)

Summary. In conclusions, the recovery of heat from the exhaust gases of an engine can lead to numerous advantages both from an economic point of view (fuel economy), once the payback time of the investment has ended, and from an environmental point of view, with consequent lower emissions of greenhouse gases and toxic atmospheric agents. The increased efficiency of the whole process, thanks to the ORC system, calculated on the efficiency of cycles with R134a and R245fa as working fluids, is about between 4% and 6% respectively. So, the cycle that provides the highest overall thermodynamic efficiency is the R245fa cycle, which also provides the highest boiler efficiency, while the R134a, cheaper than R245fa, cycle allows to have a more compact heat

exchanger (14 cm shorter than the R245fa). However, it can be notice that, due the relatively high temperatures of the exhaust gases of the engine, it is necessary to carry out experimental tests. to be absolutely sure of the safety of the "direct" configuration (although the temperatures of self-ignition of working fluids are much higher than those reached by the inner wall of the heat exchanger). The final dimensions of the heat exchanger make it suitable for vehicular applications, primarily for large vehicles such as trucks, trains and large ships. It can also be suitable for smaller vehicles (cars), but more research has to be carried out, with the aim of decreasing the dimensions, thus making the ORC for small size land vehicle applications (or even for smaller stationary applications) attractive and competitive. To further decrease the size, the heat exchanger could be subdivided in 6 or 8 smaller shells, reducing the total occupied area and then checked to eventual length reduction. However, this approach could lead to an increase in head losses. The additional use of the waste heat, deriving from the engine cooling system, to pre-heat the fluid could be efficiently advantageous, but it could be complicated, and a careful investigation is required. Finally, a CFD study could undoubtedly be useful to analyze the characteristics of the outflow along the helical tube and their effect on heat transfer and pressure drop. Besides, due to computational limitations, structural and thermal studies were carried out by dividing the heat exchanger into four basic parts. However it would be appropriate to perform a complete study on the entire heat exchanger and, in particular, on the welds lines, once the heat exchanger is assembled. In addition, with the development of new industrial fluids such as HFO 1234yf and HFO1234ze, it will be possible to considerably reduce (about 400 times) the environmental impact of such a system

Acknowledgments
This article is part of the project "Medium/Small ORC plants for industrial application", developed by the Mechanical and Aerospace Engineering Department of "Sapienza" University of Rome with the support of the private enterprise GEA S.p.A., which deserves acknowledgement from the authors.

Author Contributions
Roberto Capata dealt with the design procedure, while Giacomo Bonafoni was in charge of all aspects related to ANSYS simulations.

Conflicts of Interest
The authors declare no conflict of interest.

References
[1] Bonafoni, G. *Preliminary design of a helical coil heat exchanger for a small ORC energy recovery system*. Master Degree Thesis, Department of Mechanical & Aerospace Engineering, University of Roma "Sapienza", Rome, July 2014
[2] Wang, T.; Zhang, Y.; Peng, Z.; Shu, G. *A review of researches on thermal exhaust heat recovery with Rankine cycle*. **Renewable and sustainable energy reviews 2011**, *15*, 2862-2871.
[3] Saidur, R.; Rezaei, M.; Muzammil, W.K.; Hassan, M.H.; Paria, S.; Hasanuzzaman, M. *Technologies to recover exhaust heat from internal combustion engines*. **Renewable and sustainable energy reviews 2012,** *16*, 5649-5659.
[4] Tchanche, B.F.; Lambrinos, G.; Frangoudakis, A.; Papadakis, G. *Low-grade heat conversion into power using organic Rankine cycles–A review of various applications*. **Renewable and Sustainable Energy Reviews 2011,** 15, 3963–3979**.**
[5] Capata, R.; Sciubba, E. *A small-scale ORC energy recovery system for vehicular application: feasibility analysis and preliminary components design*. In **IMECE 2013-63410**, Proceedings of the ASME 2013 International Mechanical Engineering Congress and Exposition, San Diego, California, USA, November 15-21, 2013.
[6] Capata, R.; Sciubba, E.; Toro, C. *The gas turbine hybrid veichle Lethe at UdR1: the On-Board innovative Orc energy recovery system – feasibility analysis*. In **IMECE2012-85237**, Proceedings of the ASME 2012 International Mechanical Engineering Congress and Exposition, Houston, Texas, USA, November 9-15, 2012.

[7] Shu, G.; Yu, G.; Tian, H.; Wei, H.; Liang, X. *A Multi-Approach Evaluation System (MA-ES) of Organic Rankine Cycles (ORC) used in waste heat utilization*. **Applied Energy 2014**, *132*, 325-338.
[8] Boretti, A. *Recovery of exhaust and coolant heat with R245fa organic Rankine cycles in a hybrid passenger car with a naturally aspirated gasoline engine*. **Applied Thermal Engineering 2012**, *36*, 73-77.
[9] Wang, E.H.; Zhang, H.G.; Fan, B.Y.; Ouyang, M.G.; Zhao, Y.; Mu, Q.H. *Study of working fluid selection of Organic Rankine Cycle (ORC) for engine waste heat recovery*. **Energy 2011**, 36, 3406-3418.
[10] Toffolo, A.; Lazzaretto, A.; Manente, G.; Paci, M. *A multi-criteria approach for the optimal selection of working fluid and design parameters in Organic Rankine Cycle systems*. **Applied Energy 2014,** *121*, 219-232.
[11] National Institute of Standards and Technology. http://webbook.nist.gov/chemistry/fluid/ (accessed on 26/07/2014).
[12] Peace Software. http://www.peacesoftware.de/einigewerte/einigewerte_e.html (accessed on 3/08/2014) .
[13] Capata, R.; Hernandez, *G. Preliminary design* and simulation of a Turbo Expander for small rated power Organic Rankine Cycle (ORC). **Energies 2014**, **7 (11),** 7067-7093; doi: 10.3390/en7117067.
[14] Patil, R.K.; Shende, B.W.; Ghosh, P.K. *Designing a helical-coil heat exchanger.*, **Chemical Engineering,** 13 December 1982.
[15] Amori, K.E.; Sherza, J.S. *An investigation of shell-helical coiled tube heat exchanger used for solar water heating system.* **Innovative Systems Design and Engineering, 2013,** Vol. 4, No.15, ISSN 2222-1727 (Paper).
[16] Elsayed, A.M. *Heat Transfer in Helically Coiled Small Diameter Tubes for Miniature Cooling Systems*. PhD Thesis, The School of Mechanical Engineering, University of Birmingham, September 2011.
[17] Naphon, P.; Wongwises, S. *A review of flow and heat transfer charateristics in curved tubes*. **Renewable and Sustainable Energy Reviews 2006**, *10*, 463-490.
[18] Salimpour, M.R. *Heat transfer coefficients of shell and coiled tube heat exchangers*. **Experimental Thermal and Fluid Science, 2009**, *33*, 203-207.
[19] Kuppan, T. **Heat Exchanger Design Handbook**, 1st ed.; Marcel Dekker, Inc.: New York, NY, USA, 2000; pp. 29-41.
[20] AZoM: Materials Science and Engineering Information. http://www.azom.com/article.aspx?ArticleID=6817 (accessed on 28/08/2014).